JACS
JOURNAL OF THE AMERICAN CHEMICAL SOCIETY
Article
pubs.acs.org/JACS

Nanoscale Stabilization of New Phases in the PbTe–Sb_2Te_3 System: $Pb_mSb_{2n}Te_{m+3n}$ Nanocrystals

Ronald B. Soriano,[†] Indika U. Arachchige,[†] Christos D. Malliakas,[†] Jinsong Wu,[‡] and Mercouri G. Kanatzidis*,[†]

[†]Department of Chemistry and [‡]Department of Material Science, Northwestern University, Evanston, Illinois 60208, United States

Supporting Information

ABSTRACT: A series of novel rock-salt-type $Pb_mSb_{2n}Te_{m+3n}$ nanocrystals (m = 2, 3, 4, 6, 8, and 10; n = 1 and 2) were successfully prepared using a colloidal synthesis route. These materials are stable only on the nanoscale and have no bulk analogues. Elemental compositions were determined using scanning transmission electron microscopy/energy-dispersive X-ray spectroscopy (STEM/EDS) and inductively coupled plasma atomic emission spectroscopy (ICP-AES). The nanocrystals exhibit well-defined band energies in the mid-IR region that are nearly independent of their atomic compositions. $Pb_mSb_{2n}Te_{m+3n}$ nanocrystals behave as metastable homogeneous solid solutions at room temperature and tend to phase separate into the respective binary PbTe + Sb_2Te_3 at 300 °C. Furthermore, pair distribution function (PDF) analysis suggests that the local structure of these $Pb_mSb_{2n}Te_{m+3n}$ nanocrystals is distorted with respect to the rock-salt structure.

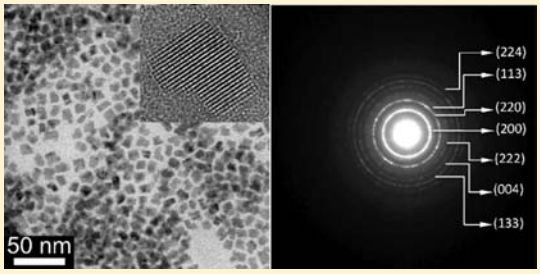

INTRODUCTION

The foundations of nanoscience are based on the premise that nanocrystalline materials behave differently than their bulk counterparts.[1−4] Electronic, optical, and physical properties can be tuned by varying the size, shape, and composition in the nanoscale regime because of the quantization of energy levels and the high surface-area-to-volume ratio.[3,5−7] For this reason, nanocrystalline materials are regarded as new materials and can impact a variety of applications including biological imaging,[8] optoelectronics,[9,10] and photovoltaics.[10,11] Much of the research is focused on the preparation of simple binary nanocrystals of semiconducting metal chalcogenides such as CdQ,[12,13] PbQ,[14,15] and Ag_2Q[16] (Q = S, Se, and Te), as well as metal and intermetallic systems containing Au, Ag, and Pt.[17−19] More complex ternary and quaternary nanocrystals can exhibit novel structures and properties, as well as enhanced functionalization ability to yield new magnetic properties, higher thermoelectric figures of merit, and the observation of band inversion.[20−22] The preparation of nanocrystals with complex compositions can be challenging because of a number of constraints including a tendency toward phase separation and the limited availability of suitable and compatible precursors in the reaction medium.[20] To date, reported ternary and quaternary nanocrystals include $AgPb_mSbTe_{m+2}$,[20,23] $AgInS_2$,[24] $CuInS_2$,[24] $CuInSe_2$,[25] $AgInSe_2$,[24] Cu_2ZnSnS_4,[26,27] and $Cu_2ZnSnSe_4$.[28]

Nearly all activity in nanoparticle science to date has focused on preparing nanocrystals of almost any known bulk phase. An unexplored frontier in this field is the possibility of stabilizing materials with compositions and structures on the nanoscale that do not exist in the bulk. This represents a new approach that has the potential to lead to entirely new nanomaterials because it is not based on the familiar paradigm of nanosizing known bulk solids.

Recently, we showed that a metastable kinetic phase of $Pb_{2-x}Sn_xS_2$ can be obtained through size reduction.[29] $Pb_{2-x}Sn_xS_2$ nanocrystals ($0.4< x <1$) with a cubic structure were obtained for compositions that are otherwise orthorhombic in the bulk. Crystal forms unlike those stable in the bulk have been observed in various semiconductors upon size reduction to the nanoscale, such as orthorhombic-type MnAs;[30] tetragonal-type Ag_2Se (β-Ag_2Se);[31] and wurtzite-type MnSe (γ-MnSe),[32] $CuInS_2$,[33] $CuInSe_2$,[34] Cu_2SnSe_3,[35] and Cu_2ZnSnS_4.[36,37] A particular example is the metastable wurtzite Cu_2SnSe_3 phase, which can be accessed instead of the stable cubic phase by varying reaction parameters such as the capping ligands and the chalcogenide source.[35]

In the mentioned examples, the composition of the nanocrystal already exists in bulk form but in a different crystal structure. Examples, however, of phases that do not exist as bulk materials but do exist as nanocrystals are few. The goal of this research is to investigate whether such novel nanomaterials could be prepared. We selected as an example the PbTe/Sb_2Te_3 system, which consists of two immiscible phases, as shown in the phase diagram of Figure 1.[38] PbTe and Sb_2Te_3 are the end members of this system and are regarded as important materials for thermoelectric applications.[39] PbTe and Sb_2Te_3 differ in the space groups in which they crystallize, namely, cubic rock-salt ($Fm\bar{3}m$) and rhombohedral ($R\bar{3}m$), respectively. The PbTe/Sb_2Te_3 system has been extensively researched by a number of groups as a candidate for thermoelectric devices by utilizing

Received: September 28, 2012
Published: December 28, 2012

   dx.doi.org/10.1021/ja309626q | J. Am. Chem. Soc. 2013, 135, 768−774

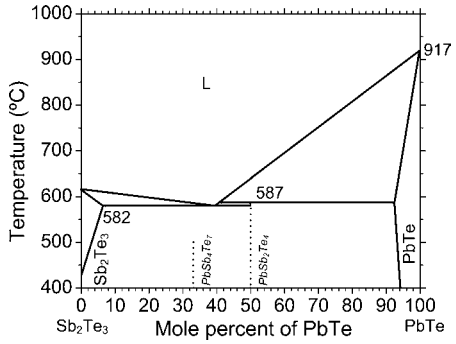

Figure 1. Schematic of the pseudobinary phase diagram of PbTe/Sb_2Te_3, showing the immiscibility of the two phases.

phase-transformation reactions such as eutectoid reactions,[40,41] precipitations,[42] and solidification.[43] The bulk PbTe/Sb_2Te_3 system always behaves as a pseudobinary system and does not form solid solutions at or near room-temperature conditions. Only two compounds (neither of which is well characterized or documented) have been reported for the entire composition range of the system, and both crystallize in the $P\bar{3}m$ space group, in complete contrast to both pure PbTe and pure Sb_2Te_3.[38]

Here, we report the preparation of new ternary nanocrystals of Pb−Sb−Te with a cubic rock-salt-type structure ($Fm\bar{3}m$) that have no bulk counterparts. Rather, these nanocrystal compositions in the bulk are mixtures of PbTe and Sb_2Te_3. We show that the nanocrystals of $Pb_mSb_{2n}Te_{m+3n}$ are single phases and not phase-segregated. The stability of these novel nanocrystals validates the concept of pursuing phases that exist only on the nanoscale but are unstable in the bulk and thus define a new class of nanomaterials. This approach diverges from the established paradigm in nanoparticle science whereby bulk materials are typically synthesized as nanocrystals.

EXPERIMENTAL SECTION

Materials. Tri-*n*-octylphosphine (TOP, 90%), tellurium powder (99.9%), 1-octadecene (90%), oleic acid (90%), oleylamine (90%), lead acetate trihydrate, antimony acetate, anhydrous ethanol, hexane, carbon tetrachloride, acetone, and ethanol were purchased from Aldrich. A 1.0 M Te/TOP solution was prepared in a nitrogen glovebox by dissolving 2.55 g (20.0 mmol) of elemental tellurium in 20 mL of TOP at 150 °C. All other chemicals were used without further purification.

Synthesis of $Pb_mSb_{2n}Te_{m+3n}$ Nanocrystals. All syntheses were carried out under air-free conditions using a Schlenk line. In a typical synthesis, stoichiometric amounts of lead acetate trihydrate and antimony acetate, 20.0 mL of octadecene, 5.00 mL of oleic acid, and 5.00 mL of oleylamine were placed in a 100 mL Schlenk flask and dried under a vacuum at 100 °C for 3−4 h to obtain a homogeneous pale yellow solution (Table S1, Supporting Information). The reaction flask was flushed with nitrogen, and the temperature was subsequently raised to 160 °C. At 160 °C, an appropriate amount of Te/TOP solution was swiftly injected (Table S1, Supporting Information). Upon injection, a dark brown colored mixture resulted. The temperature of the resulting mixture was maintained at 150−160 °C for 1 min, and the reaction mixture was then rapidly cooled to room temperature using an ice−water bath. The resulting nanocrystals were precipitated by the addition of 20.0 mL of an ethanol/hexanes (1:1) solution and an additional 20.0 mL of ethanol followed by centrifugation. A black pellet of $Pb_mSb_{2n}Te_{m+3n}$ nanocrystals was isolated by discarding the supernatant liquid. The resulting nanocrystals were resuspended in hexanes and reprecipitated with excess ethanol. The purified nanocrystals can be dispersed in nonpolar organic solvents such as hexane, chloroform, and carbon tetrachloride to form stable colloidal suspension. $Pb_mSb_{2n}Te_{m+3n}$ nanocrystals of different atomic compositions were prepared by varying the molar ratios of the Pb, Sb, and Te precursors.

Characterization. An INEL CPS120 X-ray powder diffractometer with graphite-monochromatized Cu Kα radiation was used for X-ray powder diffraction measurements. Nanocrystal samples were deposited on a glass holder coated with a thin layer of light mineral oil, and the diffraction patterns were recorded at 40 kV and 20 mA.

Nanocrystal samples for transmission electron microscopy (TEM) analysis were prepared by depositing a drop of nanocrystals suspended in anhydrous hexanes onto ultrathin carbon-coated copper grids and allowing the solvent to evaporate. TEM analyses were conducted in both dark-field and bright-field modes using a JEOL FasTEM 2100 analytical electron microscope operating at an accelerating voltage of 200 kV. Average particle sizes were manually estimated by measuring the sizes of 100−200 individual nanoparticles in several TEM images. Elemental compositions and spectral line profiles of nanocrystals were obtained using dual energy-dispersive spectroscopy (EDS) units (ThermoScientific) attached to a Hitatchi HD-2300 ultra-high-resolution field-emission scanning transmission electron microscope using a 1-nm scanning probe.

ICP measurements were carried out by dissolving nanocrystal powder in aqua regia (HNO_3/HCl, 1:3 volumetric ratio) and then diluting with ultrapure water. A Thermo Scientific Nicolet 6700 model FT-IR spectrometer was used to record the IR spectra of nanoparticles. All samples were stirred with a 0.500 M solution of hydrazine in anhydrous acetonitrile at 25 °C for 2−3 days to remove the surfactants and vacuum-dried at 25 °C for 2 days before analysis. The transmittance-versus-wavelength data collected were used to estimate the band gap of the materials by converting transmittance to absorption using the Kubelka−Munk function.[44] For annealing studies, nanocrystal powder samples were placed in quartz and annealed under a vacuum at 300 °C for 4 h.

A suspension of nanocrystals of $Pb_mSb_{2n}Te_{m+3n}$ in hexanes was sealed in a pyrex capillary (1-mm diameter), and diffraction data were collected at room temperature using the rapid-acquisition pair distribution function (RA-PDF) technique.[45] Data were collected using a Perkin-Elmer a-Si detector and ∼58 keV X-rays (λ= 0.2127 Å) at the 11-ID-B beamline at the Advanced Photon Source (Argonne National Laboratory, Argonne, IL). To improve counting statistics, 200 frames of 3 s each were collected. The data were combined and integrated using the program FIT2D.[46] Various corrections were applied to the data, such as subtraction of background (hexanes) and container, Compton and fluorescence scattering, geometric, absorption, and so on.[47] Corrections were applied using the program PDFgetX2.[48] Finally, $S(Q)$ was truncated at a Q_{max} value of 23 Å^{-1} before the PDF was calculated. Simulations and fittings were carried out using PDFfit2.[49]

RESULTS AND DISCUSSION

A series of ternary nanocrystals of the formula $Pb_mSb_{2n}Te_{m+3n}$ can be prepared by a route in which oleate salts of Sb and Pb are generated in situ and allowed to react with elemental Te dissolved in TOP. A reaction scheme of the syntheses steps is shown in Figure S2 (Supporting Information). The reactions were carried out in 1-octadecene, a high-boiling noncoordinating organic solvent. The temperature (160 °C) at which the Te solution was swiftly injected into the precursor solution was determined to be the decomposition temperature of the antimony and lead oleate salts. This temperature was optimized because, at higher temperatures, the reaction mixture started to turn into a milky white suspension as a result of the formation of Sb_2O_3. The reaction was allowed to proceed for 1 min to ensure the formation of relatively monodisperse nanocrystals of ∼10-nm size. All of the prepared $Pb_mSb_{2n}Te_{m+3n}$ nanocrystals formed highly stable colloidal suspensions. We observed that the amount of Sb incorporation could be controlled by varying

dx.doi.org/10.1021/ja309626q | J. Am. Chem. Soc. 2013, 135, 768−774

the nominal amount of the starting Sb precursor. Oleic acid and oleylamine were both used as surfactants to encourage the formation of stronger complexes with Pb^{2+} and Sb^{3+}, ultimately leading to the stabilization of Sb inside the PbTe matrix. Remarkably, we found that it is possible to incorporate large fractions of Sb to create nanoparticles in which the Sb/Pb ratio is about 2.61. In contrast, we observed that using oleic acid alone as the capping ligand resulted in the formation of spherical and highly monodisperse particles with the major drawback of poor Sb incorporation (Figures S2 and S3, Supporting Information).

The powder X-ray diffraction patterns of the as-synthesized $Pb_mSb_{2n}Te_{m+3n}$ nanocrystals show high crystallinity with the characteristic cubic rock-salt structure belonging to the $Fm\bar{3}m$ space group (Figure 2a). Furthermore, no impurity peaks

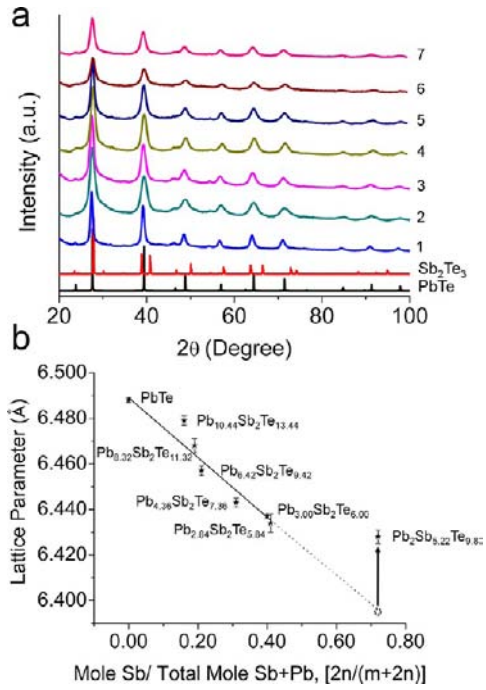

Figure 2. (a) Powder X-ray diffraction patterns of (1) $Pb_{10.44}Sb_2Te_{13.44}$, (2) $Pb_{8.32}Sb_2Te_{11.32}$, (3) $Pb_{6.42}Sb_2Te_{9.42}$, (4) $Pb_{4.36}Sb_2Te_{7.36}$, (5) $Pb_{3.00}Sb_2Te_{6.00}$, (6) $Pb_{2.84}Sb_2Te_{5.84}$, and (7) $Pb_2Sb_{5.22}Te_{9.83}$ nanocrystals. Black and red lines represent the simulated PXRD patterns of bulk PbTe (ICSD 96500) and bulk Sb_2Te_3 (ICSD 2084), respectively. (b) Change in lattice parameter as a function of increasing Sb incorporation. The system deviates from Vegard's law when the amount of Sb present exceeds the amount of Pb. A lattice expansion is observed for $Pb_2Sb_{5.22}Te_{9.83}$.

corresponding to binary Sb_2Te_3 or elemental Pb, Sb, or Te were observed, suggesting the single-phase nature of the as-prepared nanocrystals. However, a minor impurity peak at 55° (2θ) was observed and attributed to the presence of Sb_2O_3 on the surface of the prepared particles as a result of partial oxidation. Relative to that of PbTe, the diffraction patterns are shifted to larger 2θ Bragg angles consistent with shorter lattice due to incorporation of Sb atoms in the structure. The lattice parameters of $Pb_mSb_{2n}Te_{m+3n}$ nanocrystals decrease systematically with increasing Sb concentration (Figure 2b). A lattice expansion was observed for $Pb_2Sb_{5.22}Te_{9.83}$, but the reason for this is unclear. One possibility might be that the large displacements of the Sb atoms from the ideal octahedral sites result in an apparent increase of the size of this atom in the structure. The average particle sizes of the different samples were calculated based on the line broadening of Bragg reflections using the Scherrer formula[50] and found to be in the range of 9.4−12.7 nm. In addition, particles were also allowed to grow for 5 and 30 min to investigate the growth rate. We observed that the rate of growth is moderate and the particles tend to be more polydisperse with increasing reaction time, with average particle size of 13.7 ± 1.1 and 36 ± 3.5 nm for 5- and 30-min preparations, respectively (Figure S4, Supporting Information). Also, particles that were allowed to grow for 30 min indicated the beginnings of phase separation into PbTe and Sb_2Te_3. Further, attempts to prepare bulk-size particles of $Pb_mSb_{2n}Te_{m+3n}$ by allowing the reaction to proceed for 5 h indicated that the particles phase-separated into PbTe + Sb_2Te_3 (and a minor phase of Sb_2O_3), as shown in the powder X-ray diffraction pattern (Figure S5, Supporting Information). This confirms that these materials are stable only in the nanoscale size regime.

When the lattice parameters are plotted against the Sb mole fraction, a linear relationship is obtained, which indicates that Vegard's law is obeyed. However, a deviation from this trend was observed for nanocrystals containing more Sb than Pb. This can be explained by a deviation of the local structure (from the octahedral geometry) brought about by the well-known lone-pair distortion of Sb^{3+} ions, which has a tendency to be stereochemically expressed.[51,52] The latter was observed in cubic rock-salt α-$LiAsSe_2$ containing As^{3+}, which shows an average cubic rock-salt structure by Bragg scattering but like PbTe it exhibits distortions away from the ideal octahedral coordination for both Li and As atoms as confirmed by PDF analysis.[53] Therefore, to examine the local structure and the existence of short-range distortions, we performed PDF analysis on a series of $Pb_mSb_{2n}Te_{m+3n}$ nanocrystals (Figure 3). The rock-

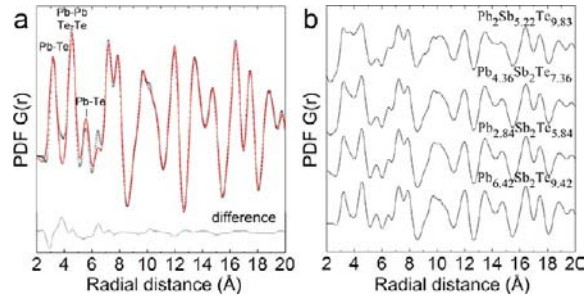

Figure 3. (a) Pair distribution function (PDF) plot of $Pb_{6.42}Sb_2Te_{9.42}$ nanocrystals. The red solid line represents the fit of the cubic PbTe model to the experimental data (open circles). Discrepancies in the local range (<7 Å) are apparent from the difference curve. Peaks were assigned relative to the rock-salt structure. (b) PDF plots of nanocrystals with different Pb/Sb ratios. Compositions rich in Pb tend to yield less locally distorted structures. With decreasing Pb/Sb ratio, the local structure becomes more distorted, as is evident from the increase in PDF intensity around 4 Å.

salt PbTe model[54] fits the experimental data very well in the mid- and long-range regions (>7 Å), but the agreement is poor in the short-range (<7 Å) region, indicative of local structural distortion (Figure 4a). The discrepancies at short range are also apparent from the difference curve in Figure 4a. Also, the PDF peaks were assigned according to the rock-salt structure, showing the nearest neighbors with corresponding intensity (Figure 4a). Interestingly, the magnitude of the local distortion was found to be different among the different members of the

dx.doi.org/10.1021/ja309626q | J. Am. Chem. Soc. 2013, 135, 768−774

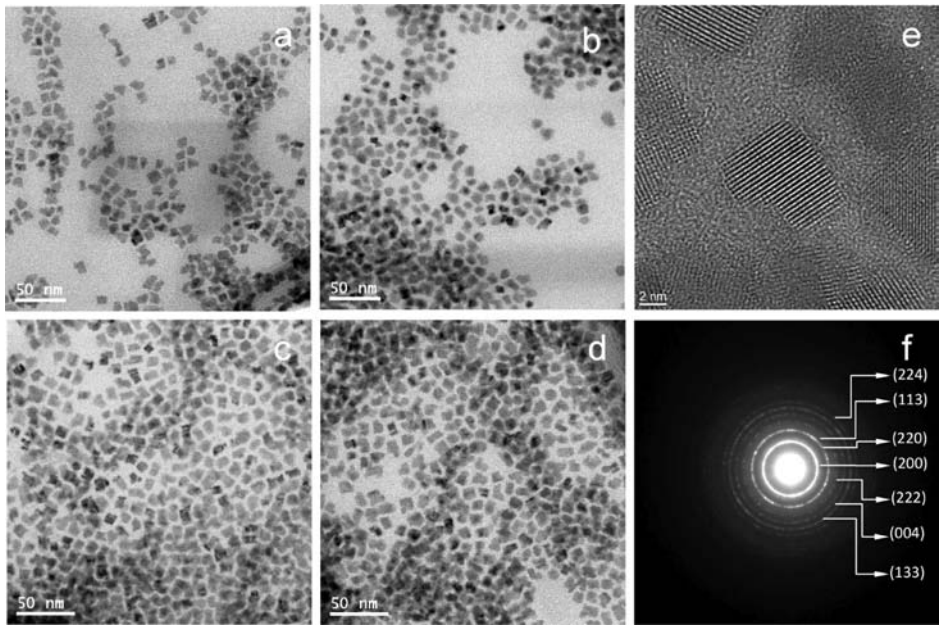

Figure 4. TEM images of as-synthesized (a) $Pb_2Sb_{5.22}Te_{9.83}$, (b) $Pb_{2.84}Sb_2Te_{5.84}$, (c) $Pb_{6.42}Sb_2Te_{9.42}$, and (d) $Pb_{10.44}Sb_2Te_{13.44}$ nanocrystals. (e) HR-TEM micrograph of the $Pb_{2.84}Sb_2Te_{5.84}$ sample, showing a regular rock-salt-type crystal structure. (f) Selected-area electron diffraction pattern from a ~200 nm × 200 nm area of a grid loaded with nanocrystals. The Bragg reflections can be indexed to the cubic $Fm\bar{3}m$ space group.

Table 1. Elemental Composition, Average Particle Size, Lattice Parameters, and Optical Band Gaps of $Pb_mSb_{2n}Te_{m+3n}$ Nanoparticles

		crystallite size (nm)			
nominal composition	actual composition (ICP-AES)	PXRD	TEM	lattice parameter (Å)	band gap (eV)
$Pb_3Sb_4Te_9$	$Pb_2Sb_{5.22}Te_{9.83}$	9.4	9.8 ± 0.5	6.428(3)	0.45
$Pb_2Sb_2Te_5$	$Pb_{2.84}Sb_2Te_{5.84}$	10.3	10.1 ± 0.5	6.434(4)	0.42
$Pb_3Sb_2Te_6$	$Pb_{3.00}Sb_2Te_{6.00}$	11.5	11.3 ± 0.6	6.437(1)	0.41
$Pb_4Sb_2Te_7$	$Pb_{4.36}Sb_2Te_{7.36}$	9.5	9.6 ± 0.8	6.443(2)	0.44
$Pb_6Sb_2Te_9$	$Pb_{6.42}Sb_2Te_{9.42}$	11.8	11.7 ± 0.8	6.457(2)	0.42
$Pb_8Sb_2Te_{11}$	$Pb_{8.32}Sb_2Te_{11.32}$	11.1	10.8 ± 0.5	6.468(3)	0.43
$Pb_{10}Sb_2Te_{13}$	$Pb_{10.44}Sb_2Te_{13.44}$	12.7	12.4 ± 0.7	6.479(2)	0.42

$Pb_mSb_{2n}Te_{m+3n}$ family examined by PDF (Figure 3b). It seems that, when the $Pb_mSb_{2n}Te_{m+3n}$ member is rich in Pb (or poor in Sb), the local structure is less distorted and structurally closer to that of cubic PbTe, as evidenced by the additional PDF intensity that appears at around 4 Å. The higher the Sb/Pb ratio the more distorted the local structure was found to be in the nanoparticles (Figure 3b).

The elemental compositions of the $Pb_mSb_{2n}Te_{m+3n}$ nanocrystals were determined using inductively coupled plasma atomic emission spectroscopy (ICP-AES). The actual compositions are close to the nominal ones, indicating the good control of composition achieved by our reaction conditions. However, attempts to obtain a composition with equal amounts of Pb and Sb starting with equimolar amounts proved to be unsuccessful. A detailed discussion regarding the elemental analysis measurements is presented in the Supporting Information. The results for the ICP-AES analysis are reported in Table 1.

Transmission electron microscopy (TEM) images of representative $Pb_mSb_{2n}Te_{m+3n}$ nanocrystals are shown in Figure 4a–d. The as-prepared nanoparticles exhibit a relatively narrow size distribution but no regular shape. This can be explained by the use of a mixture of oleic acid and oleylamine as surfactants, which have preferential affinities toward Pb and Sb and exert uneven surface passivation, leading to the observed irregularity in shape. The average particle sizes are consistent with the average crystallite size calculated from PXRD measurements and are also included in Table 1. The high-resolution TEM image of $Pb_{2.84}Sb_2Te_{5.84}$ in Figure 4e confirms the high crystallinity of the nanocrystals. Selected-area electron diffraction patterns collected from a ~200 nm × 200 nm area loaded with nanocrystals further confirm the crystalline nature and display Bragg reflections corresponding to the cubic NaCl-type structure (Figure 4f).

The presence of Pb, Sb, and Te was confirmed by recording energy-dispersive spectra using scanning transmission electron microscopy (STEM) mode with a 1-nm scanning probe. Figure 5a,b shows a typical example for a $Pb_{4.36}Sb_2Te_{7.36}$ nanocrystal sample. To confirm the single-phase homogeneity of the prepared nanocrystals, an EDS line-scan analysis was performed wherein a consistent rise and fall of Pb, Sb, and Te signals moving along a single particle is apparent from the profile (Figure 5c,d). Similar results were obtained from other compositions and demonstrate that the nanocrystals prepared through this route contained single phase rather than phase-separated particles with localized PbTe and Sb_2Te_3 domains.

Another interesting structural feature of the $Pb_mSb_{2n}Te_{m+3n}$ nanocrystals is the unequal numbers of cations (Pb^{2+} and Sb^{3+})

dx.doi.org/10.1021/ja309626q | J. Am. Chem. Soc. 2013, 135, 768–774

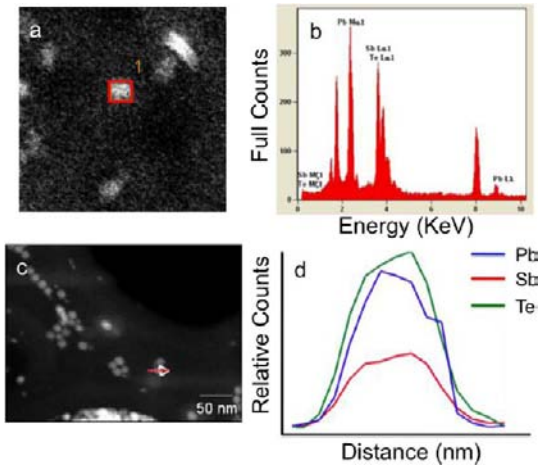

Figure 5. (a) STEM image of $Pb_{4.36}Sb_2Te_{7.36}$ nanocrystals and (b) the corresponding EDS spectrum, showing the presence of all of the expected elements in a single nanoparticle. (c) STEM image of the nanocrystals and (d) a line-scan analysis through individual particles (along the direction of the arrow in panel c), confirming the homogeneous phase behavior of the $Pb_{4.36}Sb_2Te_{7.36}$ nanocrystals.

and anions (Te^{2+}). Despite the NaCl-type structure, the metal (Pb + Sb) to nonmetal (Te) ratio is <1. This indicates the presence of massive metal vacancies in the structure. Based on the compositions, large cation vacancies (as high as 20% in $Pb_2Sb_{5.22}Te_{9.88}$) are present in the cubic structure. Evidently, so many metal vacancies cannot be supported by the bulk systems, and they naturally phase separate into the binary phases of PbTe and Sb_2Te_3. The stability of the metal vacancies in the structure on the nanoscale is surprising, and it raises the question of its origin. Are the nanocrystals kinetically stabilized during the rapid synthesis procedure, or are they thermodynamically stable because the total energy of the metal-defected NaCl structure is lowered below that of the phase-separated counterpart as the nanoparticle size is reduced? Answering this question will require state-of-the-art first-principles calculations that are beyond the scope of this work.

The $Pb_mSb_{2n}Te_{m+3n}$ nanocrystals exhibit well-defined optical band energy gaps in the mid-IR region. The band-gap onset values estimated from the absorption spectra are in the range of 0.41−0.45 eV. By comparison, the band gap of pure PbTe nanocrystals of comparable size is ∼0.43 eV. The results are included in Table 1, and representative spectra are shown in Figure 6. Presumably, these bandgaps are consistent with the expected quantum confinement effect, whereby the band-gap energies of the nanocrystals are significantly larger than those of the bulk materials. The issue in this case is the bulk band-gap values to which the nanocrystal values should be compared, as no corresponding bulk phases exist. By comparison, the bulk band gaps of the individual binary end members are 0.28 eV for PbTe and 0.11 for Sb_2Te_3.[55]

The $Pb_mSb_{2n}Te_{m+3n}$ nanocrystals tend to phase separate or segregate at moderately high temperature, such as ∼300 °C. PXRD patterns of $Pb_{2.84}Sb_2Te_{5.84}$ nanocrystals annealed at 300 °C for 4 h show the diffraction peaks of crystalline PbTe, Sb_2Te_3, and Sb_2O_3 phases, indicating phase separation (Figure 7). Further, differential thermal analysis (DTA) confirmed the temperature at which phase separation occurs, indicated by the presence of an exothermic peak at 337 °C (Figure 7, inset). The appearance of the Sb_2O_3 phase is adventitious and attributed to particle oxidation and incomplete removal of oleic

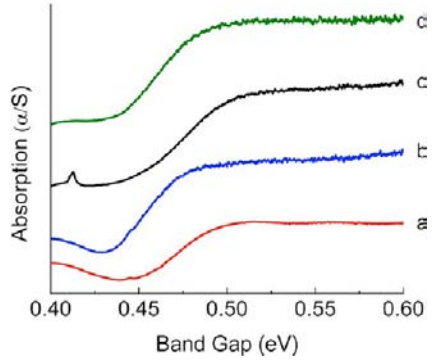

Figure 6. Infrared absorption spectra of (a) $Pb_2Sb_{5.22}Te_{9.83}$ (0.45 eV), (b) $Pb_{8.32}Sb_2Te_{11.32}$ (0.43 eV), (c) $Pb_{4.36}Sb_2Te_{7.36}$ (0.44 eV), and (d) PbTe (0.43 eV) nanocrystals, showing band gaps. All samples were stirred in a 0.5 M hydrazine solution in acetonitrile for 2 days and were then subjected to vacuum drying to remove the capping ligands.

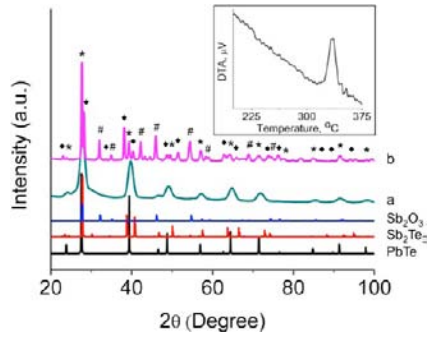

Figure 7. Powder X-ray diffraction patterns of $Pb_{2.84}Sb_2Te_{5.84}$ nanocrystals (a) as-synthesized and (b) after being annealed at 300 °C for 4 h. The diffraction peaks for pattern b are marked with *, ♦, and # corresponding to PbTe, Sb_2Te_3, and Sb_2O_3 phases, respectively. Black, red, and blue lines represent the simulated PXRD patterns of bulk PbTe (ICSD 96500), Sb_2Te_3 (ICSD 2084), and Sb_2O_3 (ICSD 240206), respectively. Inset: DTA profile showing an exothermic peak around 337 °C corresponding to the temperature at which phase separation occurs.

acid capping ligands prior to annealing of the samples. These observations suggest that the $Pb_mSb_{2n}Te_{m+3n}$ nanocrystals are either kinetically stabilized phases or thermodynamically stabilized with size being a key parameter. The fact that they decompose to the end members at higher temperatures is expected given the lack of ternary phases in the bulk PbTe/Sb_2Te_3 system.

■ CONCLUSIONS

Using a low-temperature, one-pot colloidal synthetic route, a novel series of $Pb_mSb_{2n}Te_{m+3n}$ nanoparticles that have no bulk-scale analogues can be stabilized. The ternary nanoparticles have narrow size distributions , with absorption-band onsets in the mid-IR region. The nanoparticles are solid solutions with Pb and Sb atoms and metal vacancies distributed randomly in the Na sites of the rock-salt NaCl structure. PDF analysis indicates that the local structure is distorted and that the magnitude of these distortions is proportional to the Sb/Pb ratio. The new materials undergo phase separation to PbTe and Sb_2Te_3 above 300 °C. It is significant that ternary lead−antimony−telluride materials can be stabilized exclusively in the nanoscale regime. The contrast between the bulk materials PbTe/Sb_2Te_3, which do not form rock-salt ($Fm\bar{3}m$) ternary

dx.doi.org/10.1021/ja309626q | J. Am. Chem. Soc. 2013, 135, 768−774

compounds, and the corresponding single-phase nanoparticles can serve as an excellent example that can be used to better understand the thermodynamic limits of systems as size is reduced. Further, this work suggests a heretofore little-explored avenue in nanoparticle science, and this is the pursuit of new materials that are stable only as nanoparticles.

■ ASSOCIATED CONTENT

Supporting Information

Synthesis details, X-ray diffraction data, elemental composition measurements. This material is available free of charge via the Internet at http://pubs.acs.org.

■ AUTHOR INFORMATION

Corresponding Author

m-kanatzidis@northwestern.edu

Notes

The authors declare no competing financial interest.

■ ACKNOWLEDGMENTS

This research was supported by the Office of Naval Research (Grant N00014-10-1-0331). Electron microscopy and elemental analyses were performed at the Electron Probe Instrumentation Center (EPIC) facility of the Northwestern University Atomic and Nanoscale Characterization Experimental (NUANCE) Center (supported by NSF-NSEC, NSF-MRSEC, KECK Foundation, and the State of Illinois) at Northwestern University. Use of the Advanced Photon Source, an Office of Science User Facility operated for the U.S. Department of Energy (DOE) Office of Science by Argonne National Laboratory, was supported by the U.S. DOE under Contract DE-AC02-06CH11357. R. B. Soriano is partly supported by the Hierarchical Materials Cluster Program Fellowship at Northwestern University.

■ REFERENCES

(1) Alivisatos, A. P. *Science* **1996**, *271*, 933.
(2) Murray, C. B.; Kagan, C. R.; Bawendi, M. G. *Annu. Rev. Mater. Sci.* **2000**, *30*, 545.
(3) Goldstein, A. N.; Echer, C. M.; Alivisatos, A. P. *Science* **1992**, *256*, 1425.
(4) Murray, C. B.; Norris, D. J.; Bawendi, M. G. *J. Am. Chem. Soc.* **1993**, *115*, 8706.
(5) Wang, Y.; Herron, N. *J. Phys. Chem.* **1991**, *95*, 525.
(6) Trindade, T.; O'Brien, P.; Pickett, N. L. *Chem. Mater.* **2001**, *13*, 3843.
(7) Steigerwald, M. L.; Brus, L. E. *Acc. Chem. Res.* **1990**, *23*, 183.
(8) Michalet, X.; Pinaud, F. F.; Bentolila, L. A.; Tsay, J. M.; Doose, S.; Li, J. J.; Sundaresan, G.; Wu, A. M.; Gambhir, S. S.; Weiss, S. *Science* **2005**, *307*, 538.
(9) Nazzal, A. Y.; Qu, L.; Peng, X.; Xiao, M. *Nano Lett.* **2003**, *3*, 819.
(10) Talapin, D. V.; Rogach, A. L.; Kornowski, A.; Haase, M.; Weller, H. *Nano Lett.* **2001**, *1*, 207.
(11) Huynh, W. U.; Dittmer, J. J.; Alivisatos, A. P. *Science* **2002**, *295*, 2425.
(12) Malik, M. A.; Revaprasadu, N.; O'Brien, P. *Chem. Mater.* **2001**, *13*, 913.
(13) Goldstein, A. N.; Echer, C. M.; Alivisatos, A. P. *Science* **1992**, *256*, 1425.
(14) Joo, J.; Na, H. B.; Yu, T.; Yu, J. H.; Kim, Y. W.; Wu, F.; Zhang, J. Z.; Hyeon, T. *J. Am. Chem. Soc.* **2003**, *125*, 11100.
(15) Lifshitz, E.; Bashouti, M.; Kloper, V.; Kigel, A.; Eisen, M. S.; Berger, S. *Nano Lett.* **2003**, *3*, 857.
(16) Sahu, A.; Qi, L.; Kang, M. S.; Deng, D.; Norris, D. J. *J. Am. Chem. Soc.* **2011**, *133*, 6509.
(17) Cable, R. E.; Schaak, R. E. *Chem. Mater.* **2005**, *17*, 6835.
(18) Leonard, B. M.; Bhuvanesh, N. S. P.; Schaak, R. E. *J. Am. Chem. Soc.* **2005**, *127*, 7326.
(19) Ghosh, T.; Leonard, B. M.; Zhou, Q.; DiSalvo, F. J. *Chem. Mater.* **2010**, *22*, 2190.
(20) Arachchige, I. U.; Wu, J.; Dravid, V. P.; Kanatzidis, M. G. *Adv. Mater.* **2008**, *20*, 3638.
(21) Zhao, Y.; Dyck, J. S.; Hernandez, B. M.; Burda, C. *J. Am. Chem. Soc.* **2010**, *132*, 4982.
(22) Arachchige, I. U.; Kanatzidis, M. G. *Nano Lett.* **2009**, *9*, 1583.
(23) Karkamkar Abhijeet, J.; Kanatzidis Mercouri, G. *J. Am. Chem. Soc.* **2006**, *128*, 6002.
(24) Wang, D.; Zheng, W.; Hao, C.; Peng, Q.; Li, Y. *Chem. Commun.* **2008**, 2556.
(25) Hu, J.; Lu, Q.; Tang, K.; Qian, Y.; Zhou, G.; Liu, X. *Chem. Commun.* **1999**, 1093.
(26) Steinhagen, C.; Panthani, M. G.; Akhavan, V.; Goodfellow, B.; Koo, B.; Korgel, B. A. *J. Am. Chem. Soc.* **2009**, *131*, 12554.
(27) Khare, A.; Wills, A. W.; Ammerman, L. M.; Norris, D. J.; Aydil, E. S. *Chem. Commun.* **2011**, *47*, 11721.
(28) Shavel, A.; Arbiol, J.; Cabot, A. *J. Am. Chem. Soc.* **2010**, *132*, 4514.
(29) Soriano, R. B.; Malliakas, C. D.; Wu, J.; Kanatzidis, M. G. *J. Am. Chem. Soc.* **2012**, *134*, 3228.
(30) Senevirathne, K.; Tackett, R.; Kharel, P. R.; Lawes, G.; Somaskandan, K.; Brock, S. L. *ACS Nano* **2009**, *3*, 1129.
(31) Ciucivara, A.; Sahu, B. R.; Kleinman, L. *Phys. Rev. B* **2006**, *73*, 214105/1.
(32) Sines, I. T.; Misra, R.; Schiffer, P.; Schaak, R. E. *Angew. Chem., Int. Ed.* **2010**, *49*, 4638.
(33) Pan, D.; An, L.; Sun, Z.; Hou, W.; Yang, Y.; Yang, Z.; Lu, Y. *J. Am. Chem. Soc.* **2008**, *130*, 5620.
(34) Norako, M. E.; Brutchey, R. L. *Chem. Mater.* **2010**, *22*, 1613.
(35) Norako, M. E.; Greaney, M. J.; Brutchey, R. L. *J. Am. Chem. Soc.* **2012**, *134*, 23.
(36) Lu, X.; Zhuang, Z.; Peng, Q.; Li, Y. *Chem. Commun.* **2011**, *47*, 3141.
(37) Singh, A.; Geaney, H.; Laffir, F.; Ryan, K. M. *J. Am. Chem. Soc.* **2012**, *134*, 2910.
(38) Shelimova, L. E.; Karpinskii, O. G.; Svechnikova, T. E.; Avilov, E. S.; Kretova, M. A.; Zemskov, V. S. *Inorg. Mater.* **2004**, *40*, 1264.
(39) Pinwen, Z.; Yoshio, I.; Yukihiro, I.; Yoshikazi, S.; Xiaopeng, J.; Guangtian, Z. *J. Phys.: Condens. Matter* **2005**, *17*, 7319.
(40) Ikeda, T.; Collins, L. A.; Ravi, V. A.; Gascoin, F. S.; Haile, S. M.; Snyder, G. J. *Chem. Mater.* **2007**, *19*, 763.
(41) Ikeda, T.; Ravi, V. A.; Collins, L. A.; Haile, S. M.; Snyder, G. J. *J. Electron. Mater.* **2007**, *36*, 716.
(42) Ikeda, T.; Ravi, V. A.; Snyder, G. J. *Acta Mater.* **2009**, *57*, 666.
(43) Ikeda, T.; Haile, S. M.; Ravi, V. A.; Azizgolshani, H.; Gascoin, F.; Snyder, G. J. *Acta Mater.* **2007**, *55*, 1227.
(44) (a) Liao, J. H.; Marking, G. M.; Hsu, K. F.; Matsushita, Y.; Ewbank, M. D.; Borwick, R.; Cunningham, P.; Rosker, M. J.; Kanatzidis, M. G. *J. Am. Chem. Soc.* **2003**, *125*, 9484. (b) Liao, J. H.; Varotsis, C.; Kanatzidis, M. G. *Inorg. Chem.* **1993**, *32*, 2453. (c) McCarthy, T. J.; Kanatzidis, M. G. *Chem. Mater.* **1993**, *5*, 1061. (d) Kanatzidis, M. G.; McCarthy, T. J.; Tanzer, T. A.; Chen, L. H.; Iordanidis, L.; Hogan, T.; Kannewurf, C. R.; Uher, C.; Chen, B. X. *Chem. Mater.* **1996**, *8*, 1465.
(45) Chupas, P. J.; Qiu, X. Y.; Hanson, J. C.; Lee, P. L.; Grey, C. P.; Billinge, S. J. L. *J. Appl. Crystallogr.* **2003**, *36*, 1342.
(46) Hammersley, A. P.; Svensson, S. O.; Hanfland, M.; Fitch, A. N.; Hausermann, D. *High Pressure Res.* **1996**, *14*, 235.
(47) Egami, T.; Billinge, S. J. L. *Underneath the Bragg Peaks: Structural Analysis of Complex Materials*; Pergamon Press/Elsevier: Oxford, U.K., 2003.
(48) Qiu, X.; Thompson, J. W.; Billinge, S. J. L. *J. Appl. Crystallogr.* **2004**, *37*, 678.

(49) Farrow, C. L.; Juhas, P.; Liu, J. W.; Bryndin, D.; Božin, E. S.; Bloch, J.; Th, P.; Billinge, S. J. L. *J. Phys.: Condens. Matter* **2007**, *19*, 335219.
(50) Rao, C. N. R.; Thomas, P. J.; Kulkarni, G. U. *Nanocrystals: Synthesis, Properties, and Applications*; Springer: Berlin, Germany, 2007.
(51) Makovicky, E. *Eur. J. Mineral.* **1993**, *5*, 545.
(52) Orlandi, P.; Meerschaut, A.; Palvadeau, P.; Merlino, S. *Eur. J. Mineral.* **2002**, *14*, 599.
(53) (a) Bera, T. K.; Jang, J. I.; Song, J.-H.; Malliakas, C. D.; Freeman, A. J.; Ketterson, J. B.; Kanatzidis, M. G. *J. Am. Chem. Soc.* **2010**, *132*, 3484. (b) Bozin, E. S.; Malliakas, C. D.; Souvatzis, P.; Proffen, T.; Spaldin, N. A.; Kanatzidis, M. G.; Billinge, S. J. L. *Science* **2010**, *330*, 1660−1663.
(54) Although the nanocrystals contain Sb and Pb, the electron-density contrast between Sb and Pb is negligible by X-rays. Therefore, no observable intensity difference in the PDF plots is expected.
(55) Roy, B.; Chakraborty, B. R.; Bhattacharya, R.; Dutta, A. K. *Solid State Commun.* **1978**, *25*, 617.
(56) Foley, G. M. T.; Langenberg, D. N. *Phys. Rev. B* **1977**, *15*, 4850.
(57) Park, J.-W.; Baek, S. H.; Kang, T. D.; Lee, H.; Kang, Y.-S.; Lee, T.-Y.; Suh, D.-S.; Kim, K. J.; Kim, C. K.; Khang, Y. H.; Da Silva, J. L. F.; Wei, S.-H. *Appl. Phys. Lett.* **2008**, *93*, 021914.